Royal Netherlands Institute for Sea Research

This is a preprint of:

Schulz, K.; Gerkema, T. (2018). An inversion of the estuarine circulation by sluice water discharge and its impact on suspended sediment transport. *Estuarine, Coastal and Shelf Science*, 200, 31-40

Published version: https://doi.org/10.1016/j.ecss.2017.09.031

Link NIOZ Repository: www.vliz.be/imis?module=ref&refid=293341

[Article begins on next page]

The NIOZ Repository gives free access to the digital collection of the work of the Royal Netherlands Institute for Sea Research. This archive is managed according to the principles of the Open Access Movement, and the Open Archive Initiative. Each publication should be cited to its original source - please use the reference as presented.
When using parts of, or whole publications in your own work, permission from the author(s) or copyright holder(s) is always needed.

An inversion of the estuarine circulation by sluice water discharge and its impact on suspended sediment transport

Kirstin Schulz[a,*], Theo Gerkema[a]

[a] *NIOZ Netherlands Institute for Sea Research, Department of Estuarine and Delta Systems, and Utrecht University, P.O. Box 140, 4400 AC Yerseke, The Netherlands.*

Abstract

The Wadden Sea is characterized by a complex topography of branching channels and intertidal flats, in which the interplay between fresh water discharges, wind forcing and the tidal current causes sediment transport rates and direction to be highly variable in space and time. During three field campaigns, indications of a negative estuarine circulation have been found in a channel adjacent to the coast in the Western Dutch Wadden Sea. Contrary to the classical picture of estuarine circulation, a periodic density stratification was observed that builds up during flood and breaks down during ebb. This can be related to a large freshwater source at the mouth of the channel, the sluice in Kornwerderzand. In this study, observations of this phenomenon are presented, and with the help of a numerical model the different drivers for residual suspended matter transport in this area, namely tidal asymmetries in the current velocity and the above mentioned periodic stratification, are investigated. It is found that the residual current in the area of interest points in ebb direction, caused by both the elongated ebb flow phase and the periodic stratification. On the contrary, the stronger flood currents cause a transport of suspended matter in flood direction. This transport is counteracted and therefore diminished by the effects of the sluice discharge.

*Corresponding author
Email address: kirstin.schulz@nioz.nl (Kirstin Schulz)

Keywords: inverse estuaries, SPM transport, Wadden Sea, Mud Motor

1. Introduction

Circulation patterns and the transport of suspended sediment in estuaries and coastal areas are often strongly influenced by the presence of density gradients. In the classical picture of estuarine circulation, a horizontal density gradient imposed by river run-off causes an alternation between stratified conditions during ebb flow, when light water is advected on top of dense water, and a destabilization of the water column during flood, when dense water is transported on top of lighter water. This tidal modulation is known as strain-induced periodic stratification (SIPS) [1]. The changes in the vertical density structure over the tidal cycle have implications on mixing: During the less stratified flood phase, turbulent diffusivities are increased compared to the stratified ebb phase, leading to a rather homogeneous current velocity profile during flood, and a more sheared velocity profile during ebb. This tidal asymmetry induces a two-layered residual current that is directed landwards near the bottom, and seawards near the surface. This reinforces the gravitationally driven residual current and causes a net import of suspended sediment into the estuary [e.g. 2, 3]. The asymmetry in turbulent diffusivity in the tidal cycle also affects resuspension and upward mixing of sediment. The larger diffusivities during the flood phase lead to enhanced concentrations of suspended particulate matter (SPM) in the water column, which induces an additional inward transport of sediment, referred to as tidal pumping [4]. This mechanism often dominates over the mean advective transport of suspended matter that is induced by asymmetries in the tidal flow and the resulting residual current [5]. It was found that already slight increases in salinity stratification can significantly reduce vertical mixing, hence small variations in the vertical density structure over the tidal cycle can already affect the residual sediment transport [6].

In regions characterized by high evaporation rates that dominate over rainfall and river-runoff, the density gradient in estuaries as described above can be

reversed. Evaporation has the highest effects on salinity in the shallower parts, and consequently maximum salinities occur further upstream in the estuary. This reverses the mechanisms described above and creates an inverse (or negative) estuarine circulation that typically causes sediment export [7, 8, and the references therein]. This evaporation-dominated stratification can be found in arid regions like Australia, Senegal and California, among others. Other examples of inverse estuaries, in this case caused by the intrusion of relatively fresh water masses through the mouth into the estuary during downwelling events, were observed in Spain, namely in the Ria of Pontevedra [9] and the Ria de Vigo [10]. In the York river and other rivers in the Chesapeake Bay system (North America), an interruption of the normal two-layered estuarine circulation by the advection of relatively fresh water into the river mouth has been observed during spring tide. This advection was caused by a horizontal salinity gradient along the Chesapeake Bay combined with differences in the tidal phase between the river and the bay [11]. To our knowledge, the effects of a fresh water source at the mouth of an estuary on sediment transport have not been investigated so far.

In this study, we fill this gap by a combination of field measurements and numerical modeling. Ship-based investigations of stratification, sediment transport and the circulation during a tidal cycle were performed in a channel in the Dutch Wadden Sea (Fig. 1). Evaporation effects are negligible in the Wadden Sea, lateral density gradients are formed by fresh water discharge from several sluices [12]. In particular, a sluice near the mouth of the investigated channel provides a large supply of fresh water that is advected along the coast and into the channel with the flood current, causing a periodic vertical stratification that is typical for an inverse estuary. Observations of this phenomenon from three cruises and results from an idealized numerical model are analyzed here to study the effect of this periodic stratification in comparison to other drivers for residual sediment transport (e.g. asymmetries in the tidal current). To our knowledge, this is the first extensive study on inverse estuarine circulation not caused by evaporation effects or intermittent events and its implications on

sediment transport.

Sediment transport is of special interest in this region for another reason: The investigated channel is located near the port of Harlingen, where a pilot project for an alternative location of spreading of dredged material was started in 2016. Sediment accumulation in the port of Harlingen demands frequent maintenance dredging of approximately 200,000 m^3 of fine grained sediment per year. In the context of the pilot study mentioned above (the so-called Mud-Motor project), this sediment is now partly deposited farther into the channel, away from the harbor of Harlingen, to establish a semi-continuous sediment source with the aim to nourish the adjacent salt marshes and reduce the recirculation of sediment into the harbor [see Fig. 1, and 13]. A detailed investigation of the fate of the disposed sediment and an analysis of the governing processes is needed to assess the functionality of the Mud-Motor and its possible applicability elsewhere. This includes the influence of nearby fresh water discharge on the transport of suspended sediment in the channel, which is investigated in this study.

Starting with a description of the study site, details on the data acquisition and processing are summarized in section 2. The section is complemented with a brief description of the numerical model that is used for the investigation of the factors determining the transport of water and SPM. In section 3 the observations are presented and the input data for the numerical model are derived. The model results are then presented in section 4, followed by a discussion in section 5 and the conclusions in section 6.

2. Study Site and Methods

2.1. Study Site

With an extent of approximately 10,000 km^2, the Wadden Sea forms the world's largest unbroken system of tidal flats. The barrier islands separating the Wadden Sea from the North Sea span a distance of nearly 500 km from the northern coast of the Netherlands to the Danish North Sea coast. The tidal

inlets between the islands are part of a complex system of branching channels, sand and mud flats and salt marshes near the coast [14].

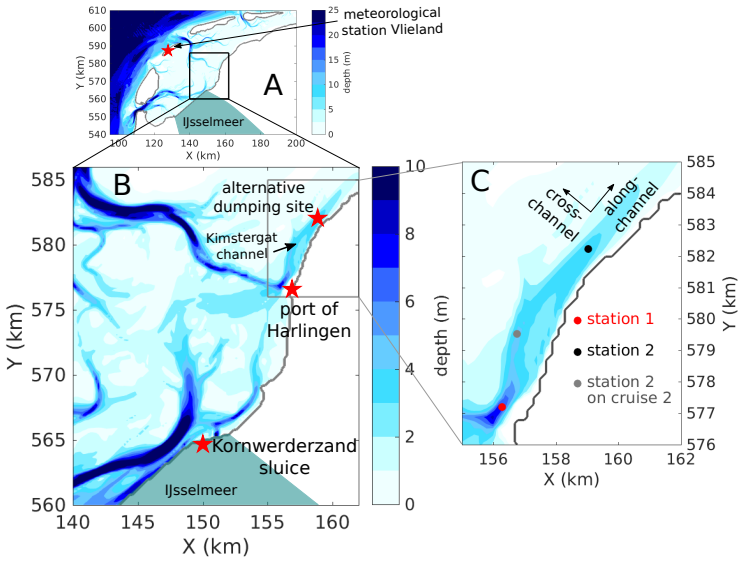

Figure 1: Bathymetric map of (a) the Dutch Wadden Sea, and (b),(c) enlargements of the study area. Please note that Rijksdriehoeks coordinates were used here, as this local projection is more accurate in the region of interest [see 15, and www.epsg.org]. Geographical coordinates of the stations are given in Tab. 1

The area investigated in this study is located in the western Dutch Wadden Sea, near the port of Harlingen (see Fig. 1). A channel parallel to the coastline (the Kimstergat, see Fig. 1b,c) connects the deep water near the port to the shallow watershed with adjacent tidal flats further to the North. The shallow end of the channel does not fall completely dry during low water, and the adjacent watershed is connected to other tidal channels. It should be kept in mind that in this respect the investigated channel is not a classical estuary.

Close to the study site, the sluice in Kornwerderzand forms one of the main fresh water sources of the Wadden Sea. It connects the Wadden Sea and the IJsselmeer, a fresh water lake artificially separated from the Wadden Sea by the building of the Afsluitdijk in 1932. At low tides, up to 2000 m^3 s^{-1} (yearly average: 200 m^3 s^{-1}) of fresh water is discharged through this sluice [14, 12].

In Fig. S1, the instantaneous discharge is displayed for the period of the first cruise that was carried out for this study. Water discharge starts during the ebb phase, when the surface elevation reaches its mean level, and is stops again approximately 5 hours later. The total discharge during one tidal cycle ranges from no discharge at all to over 30×10^6 m^3. Besides, there is a much smaller discharge from the adjacent harbor of Harlingen, at the annual mean of less than 5 m^3 s^{-1}.

2.2. Instrumentation

Measurements were performed on three cruises with the R/V Navicula in 2015 and 2016, capturing time series over a full tidal cycle near the port of Harlingen (named station 1 hereafter) and further into the Kimstergat channel (station 2) on each cruise (see Fig. 1c and Tab. 1). These stations are approximately 6 km apart, and were sampled either on two consecutive days or one day apart. The measurements were simultaneously collected from the anchored ship and from a nearby mooring (at a distance of less than 100 m from the ship). Current velocity profiles were obtained with a bottom mounted (upward facing) acoustic doppler current profiler (ADCP, Signature1000 from Nortek AS), measuring with a frequency of 8 Hz in bursts of 1 minute every 5 minutes. The bin size was set to 0.2 m with a blanking distance of 0.1 m and a mounting height of approximately 1.4 m. This allowed the ADCP to sample the water column from 1.5 m above the bottom to the surface. These data were complemented with a vessel mounted (downward facing) 1.2 kHz RDI Workhorse ADCP mounted on a pole attached to the ship. The bin size was 0.2 m, profiles were taken from 1.25 m below the surface (including the 0.25 m blanking distance) in intervals of 3 s. Both data sets were averaged over 5 minute intervals and the arithmetic mean of both sets was taken where the data overlapped. Gaps in the data that occurred at very low sea level at station 2 were interpolated [see 16, for details on the interpolation technique]. The pressure sensor of the bottom mounted ADCP was used to obtain variations in the sea surface elevation.

Vertical profiles of temperature, salinity and turbidity were measured at

cruise 1	station 1	station 2
date	16.06.2015	17.06.2015
time (UTC)	04:15 - 16:45	04:15 - 16:45
mooring position	53°10.912 N	53°13.637 N
	05°24.534 E	05°27.231 E
in RD coordinates	156450, 577243	159172, 582299
wind direction	north, stable	south-west
wind speed	low (< 5 m/s)	high (> 10 m/s)
air temperature	12-14°C	14-16°C
cruise 2	station 1	station 2
date	19.04.2016	21.04.2016
time (UTC)	04:45 - 17:15	04:00 - 16:30
mooring position	53°10.944 N	53°13.660 N
	05°24.399 E	05°26.896 E
in RD coordinates	156300, 577302	159077, 582341
wind direction	west to north	east to north
wind speed	intermediate (5-10 m/s)	low (< 5 m/s)
air temperature	9-10°C	4-11°C
cruise 3	station 1	station 2
date	25.10.2016	27.10.2016
time (UTC)	04:15 - 16:45	06:00 - 18:30
mooring position	53°10.910 N	53°13.630 N
	05°24.341 E	05°26.930 E
in RD coordinates	156235, 577240	159115, 582286
wind direction	east to south	west
wind speed	low (< 5 m/s)	intermediate (5-10 m/s)
air temperature	8-12°C	13-15°C

Table 1: Deployment times and meteorological conditions at station 1 and station 2. Start and end time refer to the parts of the data that were used for the analysis. Meteorologic data was taken from the Vlieland meteorologic station of the Royal Netherlands Meteorological Institute (KNMI). The wind direction indicates the direction from which the wind blows. RD coordinates refer to a standard geodetic coordinate system used in the Netherlands.

24 Hz with a CTD (SBE911plus, Sea-Bird Scientific) and two optical backscatter sensors (OBS, Seapoint Turbidity Meter, Seapoint Sensors Inc.). The instruments were attached to a frame that was lowered and hoisted from the stern of the ship in intervals of 20 minutes (15 minutes during cruise 3). Obtained data were directly displayed on board and the intervals were shortened whenever the optical backscatter revealed a high temporal variability. Unreasonable data from the OBS (most likely originating from mud or seaweed temporarily blocking the sensor) were removed and interpolated. Salinity was measured using the Practical Salinity Scale. Calculations were carried out using the TEOS-10 equations for sea water [17, and www.teos-10.org].

All data sets were interpolated to the same 15 minute temporal and 0.2 m vertical resolution grid for further analysis. Temporal averages were calculated at constant levels above the sea bed, which means that values in the uppermost part of the water column rely on a smaller number of data points, as water is only present there during a short period of the tidal cycle (maximal high water). This should be kept in mind when regarding the tidally averaged values in the upper part of the water column, for example in Figs. 3, 8.

2.3. SPM samples

To translate the optical backscatter data to values of suspended particulate matter concentration, two water samples using a Niskin bottle were taken every 20 min (30 min on cruise 3), one near the surface and one near the bottom. Subsamples were filtered on dried and pre-weighed GF/F filters, which were subsequently again dried and weighed to obtain the concentration of SPM. Simultaneously, OBS values for the same water sample were obtained using an OBS sensor in a dark box on board of the ship. A linear regression between the two data sets was obtained with the Theil-Sen method, which is less sensitive to outliers and therefore more appropriate in this context than the least squares fit [18]. By way of example, data and the regression for cruise 3 are displayed in Fig. S2, the linear regressions for all cruises are summarized in Tab. 2.

The calibration of the OBS sensor in the box and the one measuring in-situ

	station 1	station 2
cruise 1	$c = 770b - 10$	$c = 838b - 15$
cruise 2	$c = 807b - 16$	$c = 677b - 4$
cruise 3	$c = 720b - 2.5$	$c = 703b - 4.5$

Table 2: Linear fits between measured SPM concentration c (in $\mathrm{g\,m^{-3}}$) and OBS values b (in V).

attached to the frame was found to be very stable [19], therefore the linear correlation of $b_{\mathrm{box}} = 2.01 b_{\mathrm{frame}} - 0.01$, obtained in the laboratory after the second cruise, is used for all deployments. Details of this procedure can be found in [19, 20].

2.4. Model description

In the present study, the water column model GOTM [General Ocean Turbulence Model, see http://www.gotm.net and 21] is applied to calculate the interaction of currents, turbulent energy and salinity stratification. Several turbulence closure schemes are implemented in this model, including the $k - \varepsilon$ model that solves the transport equations for the turbulent kinetic energy k and turbulent dissipation ε. In [22], this model, together with the second-moment closure suggested by [23], was already applied for idealized studies carried out to investigate sediment transport in the Wadden Sea, and is therefore also used here.

An SPM model is coupled to the water column model via FABM (Framework for Aquatic Biogeochemial Models). A single class of SPM with constant settling velocity is used here, and the evolution of the concentration c is calculated with a simple advection-diffusion equation of the form

$$\frac{\partial c}{\partial t} = -\frac{\partial}{\partial z}(F_z - c w_s), \tag{1}$$

where w_s is the constant settling velocity, t denotes the time and z the vertical coordinate, pointing upwards from the bottom. F_z is the vertical turbulent flux

of SPM, defined as

$$F_z = -\nu_t^b \frac{\partial c}{\partial z}, \tag{2}$$

where ν_t^b is the turbulent diffusivity of buoyancy computed by the turbulence model, and equals the erosion flux at the bottom:

$$F_z = \alpha_e \max\left\{\frac{|\tau_b|}{\tau_c} - 1, 0\right\}^{1.5} \quad \text{for} \quad z = 0. \tag{3}$$

This formulation with an exponent of 1.5 reflects the typical conditions of silt/mud erosion in the Dutch Wadden Sea [e.g. 24]. The erosion constant α_e, the critical shear stress τ_c and the settling velocity w_s are the only three input parameters for the SPM model. The bottom shear stress τ_b is calculated by the water column model. Additionally, during phases when erosion occurs, sediment concentrations at the bottom are extrapolated from the concentration in the lowermost grid cell using a Rouse profile (i.e., assuming equilibrium of upward mixing and downward sinking of suspended material). This technique significantly reduces sensitivity to the grid resolution and improves numerical convergence and accuracy of the SPM model compared to implementations where the SPM concentration in the lowermost grid cell is taken as the bottom concentration. Details on the derivation of this extrapolation and the improvement of the numerical convergence can be found in [25, Appendix A].

Input parameters for both the SPM model and the water column model are derived in section 3.3 from the observations presented in the next section.

3. Observations

3.1. Transport of Suspended Matter

To gain insight into the intra-tidal dynamics in the Kimstergat channel, the temporal evolution of the along-channel current u, concentration of suspended matter and salinity distribution at station 1, measured during cruise 2, are displayed in Fig. 2. This is the deployment that exhibits the largest vertical salinity gradient at station 1, on which the model study in section 4 will be

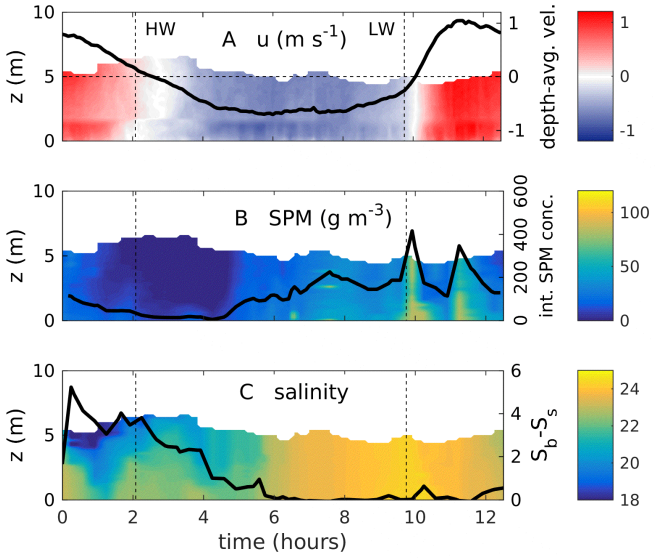

Figure 2: Evolution of (a) along-channel velocity (positive pointing to NNE, flood direction) and the depth-averaged velocity (black line), (b) SPM concentration and vertically integrated SPM concentration (black line, in gm^{-2}) (c) salinity and the difference in surface (S_s) and bottom (S_b) salinity (black line). The vertical dashed lines mark the time of high water (HW) and low water (LW), respectively. Data were obtained on cruise 2, at station 1. Here, time is reset to start at zero at the beginning of the measurements, for convenience. The original start and end times can be found in Tab. 1.

focused. Data from all other deployments are shown in the supplemental figures (Fig. S3 to Fig. S7).

Along-channel currents, with positive meaning into the channel (to the NNE, see Fig. 1), reach velocities up to 1 m s^{-1}. Maximal ebb currents occur halfway between high and low water and maximum flood currents halfway between low water and high water. The ebb phase lasts slightly longer (approximately 7.5 h) and current velocities are higher during flood. These asymmetries in the current can be found in all obtained data sets, which gives evidence of a persistent asymmetry in the tidal motion in this region. During this deployment, as well as others (see Figs. S3, S5, S7), the higher flood currents are also reflected in higher SPM concentrations during the flood phase. It is worth noting that

although the cross-channel velocities (not shown) range in the order of two magnitudes smaller than the along-channel velocities, they are directed onshore for most of the time. This induces a cross-channel SPM transport that is not negligible (see Tab. 3).[1]

Another remarkable feature is the temporal evolution of salinity stratification, visible in Fig. 2c. During the flood phase, a vertical gradient in the salinity between surface and bottom water is established, and vanishes again in the first half of the ebb period. The difference between surface and bottom salinity is up to 5 at station 1, higher than at station 2 which is further into the channel and shallower. At station 2, a top to bottom salinity difference of up to 1 is observed. Although this difference is rather small, it is good to keep in mind that [6] found that even a weak periodic salinity stratification (in the order of 1-3) can have effects on the residual transport of SPM.

The structure of the periodic stratification observed at both station 1 and 2 is opposite to what is expected in a normal estuary, where freshwater enters with ebb and periodically occurring stratification is therefore created during ebb flow and destroyed during flood. A detailed discussion of this inverse SIPS follows in section 3.2.

In Fig. 3, the vertical structure of the residual along-channel current and SPM flux are displayed for all deployments. The two-layered structure of the residual current (Fig. 3a) points in the ebb direction near the bottom for nearly all deployments.[2] This is again inverse to the classical picture of estuarine circulation, in which the residual near-bottom flow is orientated in flood direction, and motivated the further investigation of density stratification effects on the tidal current which will be described in section 4. The residual SPM flux, however, is in the flood direction for all measurements (Fig. 3b).

[1] This does not apply for station 2 on cruise 2, which was located closer to the port of Harlingen. The cross-channel transport was directed offshore, presumably caused by the curvature of the channel at the deployment position.

[2] Except at station 2, cruise 1 (solid blue line), when strong winds from the south-west were present, suggesting that this anomaly is related to the meteorological conditions.

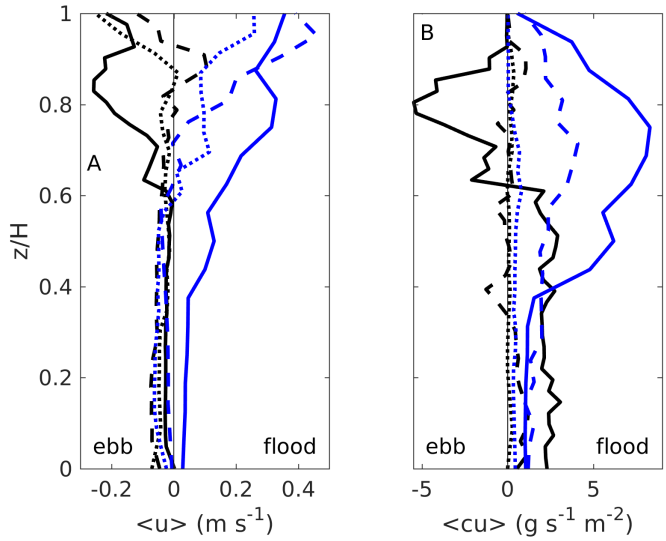

Figure 3: Vertical profiles of (a) the residual current and (b) the residual SPM flux, for all cruises. Solid lines refer to measurements from cruise 1, dashed line to cruise 2 and dotted lines to cruise 3, respectively. Black lines refer to station 1, blue lines to station 2. $< . >$ denotes the tidal average. For a better comparison, the vertical coordinate was normalized with the maximal water depth H for each deployment.

In Tab. 3 and Fig. S8, the along- and cross-channel SPM fluxes are summarized and displayed, respectively. The fluxes at station 1 (near the port of Harlingen) are rather variable, both in magnitude and vectorial direction. However, the along-channel transport is always in the flood direction, even if it is small compared to the cross-channel transport. Further into the channel, at station 2, the transport is generally more pronounced in the flood direction and onshore except for one deployment (cruise 2, Tab. 3). Although the magnitude of the SPM fluxes differs among the cruises, the main SPM transport directions are rather consistent at station 2 (see also Fig. S8).

The generally lower transport rates during cruise 3 are a result of reduced SPM concentrations in the water column. A possible cause for the reduced concentrations might be that no sediment dredging and disposal took place prior to or during the measurements at that time, as the dredging ship was

	station 1		station 2	
	along	cross	along	cross
cruise 1	5.4	1.0	12.8	−3.2
cruise 2	1.9	−1.2	9.4	1.0
cruise 3	0.5	−0.7	1.7	−0.2

Table 3: Along- and cross-channel integrated sediment flux for all cruises and both station. All values are in g s^{-1} m^{-1}. Positive values in the cross-channel component mean off-shore transport.

under maintenance.

3.2. Temporal Evolution of Salinity

As already mentioned in section 2.1, the study site is in the immediate vicinity of a large fresh water source: the Afsluitdijk sluice in Kornwerderzand (Fig. 1). Fresh water from the IJsselmeer can only be discharged when the outside sea level is low, i.e. after ebb. Subsequently, during flood, this fresh water body is pushed into the channel (the size of the flux is expected to depend also on the wind). In other words, fresh water enters at the mouth of the channel here, rather than at the back of the channel, as is usually the case with a riverine estuary. This mechanism could explain the unusual periodic stratification mentioned in the previous section and is now investigated further.

To examine the temporal variability of the vertical density stratification in detail, time series of the bulk Richardson number Ri_b are calculated for each deployment. The bulk Richardson number is a measure for the magnitude of stratification and is here defined as

$$Ri_b = \frac{g\beta\Delta\rho H^2}{U_0^2}, \tag{4}$$

where g is the acceleration of gravity, β is the saline expansivity, $\Delta\rho$ the difference in fluid density between surface and bottom, H is the water depth and U_0 the maximal depth-averaged tidal velocity [26]. The quantities ρ and β were calculated from the observations of salinity, temperature, and pressure, although density fluctuations are mainly determined by salinity differences here.

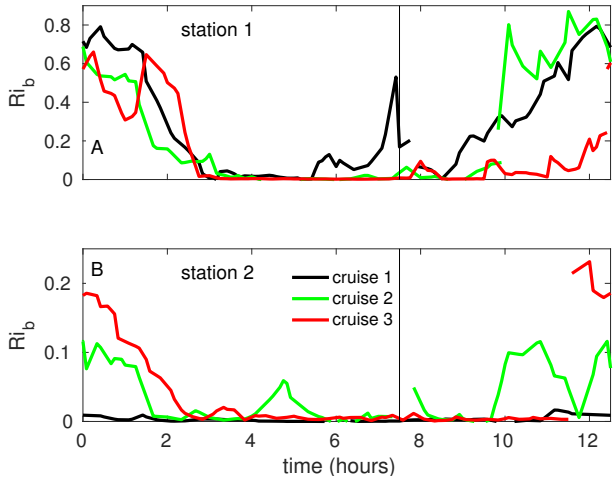

Figure 4: Temporal evolution of the bulk Richardson number Ri_b at (a) station 1 and (b) station 2 for all three cruises. For better comparison, the data sets were aligned with the onset of ebb phase, or slack tide after flood. The vertical line marks the approximate end of the ebb phase, 7.5 hours after ebb started.

The temporal evolution of Ri_b for all deployments is displayed in Fig. 4. It is visible that stratification is built up with the onset of flood (after approximately 7.5 hours in Fig. 4) and subsequently destroyed within the first 3 hours of of ebb in most cases. Absolute values of Ri_b are higher at station 1, where the vertical salinity gradients are about 4 times higher. Stratification is generally very weak at station 2, but exhibits a similar variability over the tidal cycle as at station 1. The permanently well-mixed water column at station 2 during cruise 1 (black line in Fig. 4b) was presumably created by the high wind speeds present during that deployment.

The interaction of the observed periodic stratification with the tidal current is expected to induce a residual circulation that is inverse to the dynamics in normal stratified estuaries [e.g. 26, 2]. The orientation of the residual near bottom currents, shown in the last section in Fig. 3a, supports this idea. A further analysis of the observed stratification variability effects on the tidal current and suspended matter transport will be performed with the help of a numerical model in section 4.

3.3. Derivation of Model Parameters

In this section, input data for the model described in section 2.4 are derived from observations of the surface elevation η, the depth-averaged velocity U and salinity S. The calculation of time series for η and U is straightforward: for each of the two stations, observational data from all three cruises, aligned with the onset of ebb, are averaged. Where necessary, the data were interpolated with a third order polynomial function to avoid unsteadiness (back solid lines in Fig. 5). This forcing method, hereafter referred to as 'realistic forcing', reflects the observed asymmetries in the tidal current and the surface elevation. For comparison, a fictitious forcing method, referred to as 'symmetric forcing', is created by a purely sinusoidal representation of the surface elevation and the tidal current, with an amplitude that resembles the observed extent of each property (black dashed lines in Fig. 5). This method excludes tidal asymmetries and will be comparatively used to investigate the impact of the observed asymmetries in section 4.2. The cross-channel velocity v was set to zero for all model calculations.

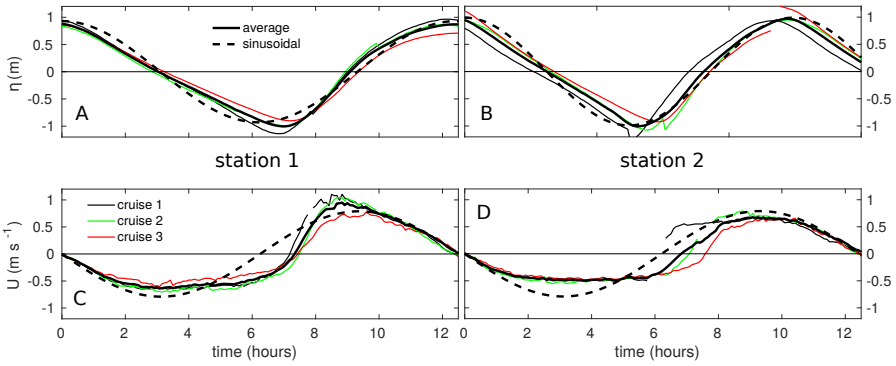

Figure 5: (a, b) Surface elevation η and (c, d) depth-averaged velocity U at station 1 (a, c) and 2 (b, d) for all three cruises (colored lines), averaged over all cruises (black lines) and a sinusoidal function of similar maximal amplitude (dashed lines). Where the averaged data was unsteady (end of deployments), cubic splines were used to interpolate 1-2 hours of the data.

To parameterize the variable salinity stratification, an arctan-shape of the

vertical salinity profile of the form

$$S(z,t) = -\frac{\Delta S(t)}{\pi} \arctan\left\{a\left(z - \frac{(H+\eta(t))}{2}\right)\right\} - b(t) \tag{5}$$

with

$$b(t) = \frac{\Delta S(t)}{\pi} \arctan\left(a\frac{(H+\eta(t))}{2}\right) - S_0 \tag{6}$$

is used. The profile depends on the mean water depth H and the (temporary variable) surface elevation $\eta(t)$. The scaling factor a was set to $a = 0.7$, which well reproduced the shape of the salinity profiles. The shift of the argument about $0.5(H+\eta(t))$ aligns the center of the profile (where the curvature changes sign) in the middle of the water column. The function $b(t)$ sets the bottom salinity of the profile to S_0.

The temporal evolution of salinity is then determined by the factor $\Delta S(t)$, which is the (asymptotic) salinity gradient of the profile:

$$\lim_{z\to\infty} (S(t,z) - S(t,-z)) = -\Delta S. \tag{7}$$

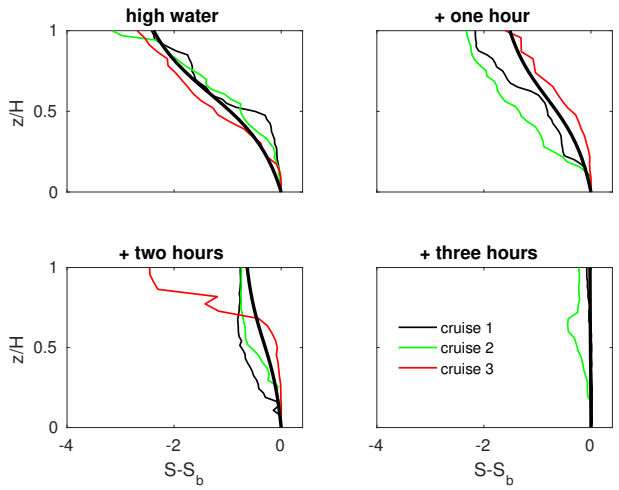

Figure 6: Observational salinity profiles at station 1 (each averaged over one hour, or 4 profiles) at high water and for the consecutive three hours, and the salinity parametrization determined by equations (5) and (8) (thick black lines). The profiles are aligned by subtracting the bottom salinity S_b for each profile.

In Fig. 6, a comparison of the observed and parameterized (equations (5) and (8)) destruction of stratification after high water at station 1 for all three cruises is displayed. The evolution of the salinity gradient over one tidal period is determined by

$$\Delta S(t) = \begin{cases} \text{linearly decreasing from max to 0} & 0 \leq t \leq 3 \\ \text{constant 0} & 3 \leq t \leq 7.5 \\ \text{linearly increasing from 0 to max} & 7.5 \leq t \leq 12.5, \end{cases} \tag{8}$$

where t is the time in hours. A maximal value of max = 4 is used for station 1[3]. In the model setup forced with the idealized symmetric tide, the ebb phase is not elongated and the onset of flood (and consequently the increase of ΔS) is therefore set to start exactly half a period after the onset of ebb. The relaxation timescale for the bulk salinity in the numerical model was set to 1 s to ensure that the prescribed salinity is directly reflected in the numerical model. The bottom salinity is set to $S_0 = 25$.

The parameters for the SPM model cannot be derived from the observations. Therefore, a sensitivity study for the three input parameters (settling velocity, critical erosion threshold and erosion constant) was conducted to determine the set of parameters that reproduced the data. A similar sensitivity analysis for a three-dimensional numerical model of the Dutch Wadden Sea was performed in [24] and the same ranges of values are used here. Comparing time series of the integrated sediment concentration of both obtained data and the different modeled concentrations showed that parameters for the suspended sediment model of $w_s = 1 \times 10^{-3}$ m s^{-1}, $\tau_c = 2.5 \times 10^{-4}$ m^2 s^{-2} reproduced the data qualitatively. Small changes in the values for these input parameters do not significantly affect the model outcome, therefore a more advanced determination of the input parameters is not necessary, regarding the idealized character of this model study. As the the overall magnitude of the SPM concentration differs a

[3]A mathematical constraint is $\Delta S \neq 0$. The 0 values in Eq. (8) therefore refer to 'very small' values in reality.

lot among the cruises (extremely low concentrations during cruise 3), the erosion constant α_e was adjusted for each cruise separately. We found that values of $\alpha_e = 2$, 1.5, and 0.2×10^{-6} kg s^{-1} m^{-2} for cruises 1,2, and 3, respectively, reproduced the SPM concentration quantitatively at station 1 (Fig. S9, S10). At station 2, $\alpha_e = 3 \times 10^{-6}$ kg s^{-1} m^{-2} for cruises 1 and 2, and $\alpha_e = 0.2 \times 10^{-6}$ kg s^{-1} m^{-2} for cruise 3 were found. In the qualitative analysis of the model results we used the erosion constant determined for the second cruise at station 1, $\alpha_e = 1.5 \times 10^{-6}$ kg s^{-1} m^{-2}, as this parameter only determines the absolute magnitude of SPM concentration and does not affect the qualitative variability, neither in the vertical nor over the tidal cycle. As in [24], bottom roughness z_0 was set to be constant with a value of $z_0 = 1.7 \times 10^{-3}$ m.

To ensure numerical convergence of the SPM model, a sensitivity analysis for the vertical and temporal resolution was carried out for sediment with a settling velocity of $w_s = 10^{-3}$ m s^{-1}. We used 150 vertical layers, strongly refined near the bottom, and a time step of 0.1 s. Runs with finer grids differed in less than 1 % in the vertically integrated sediment concentration. Therefore, this resolution and the parameters for the SPM model summarized above will be used for all simulations in section 4. To reach periodical stationarity, a spin-up time of 10 tidal periods is applied.

4. Model Results

4.1. Reproduction of Observations

To test the model setup, the realistic depth-averaged velocity and surface elevation derived in section 3.3 are used to force the model. Only the results for station 1 are displayed here, as the periodic salinity stratification is more pronounced than at station 2. A similar figure showing the results for station 2 can be found in the supplemental material (Fig. S11). The values for the input parameters are found in section 3.3.

The model outcome is displayed in Fig. 7. The along-channel velocity u (Fig. 7a) is a direct result of the model forcing and therefore well reproduces

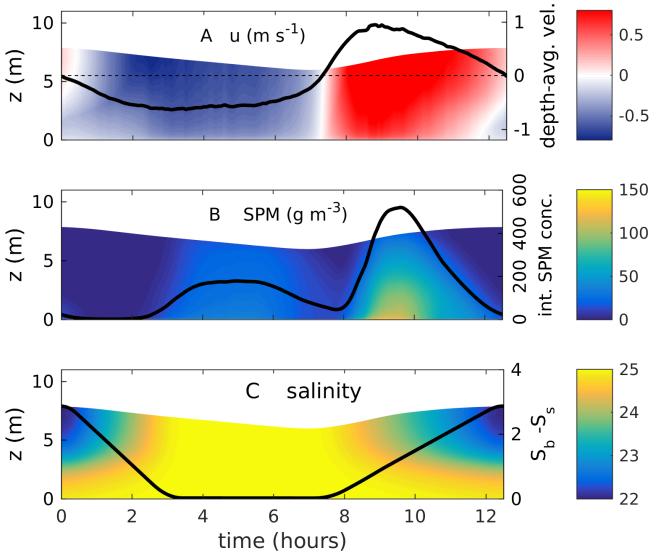

Figure 7: Temporal evolution of (a) the along-channel and depth-averaged (black line) velocity, (b) SPM concentration and integrated concentration (black line), and (c) salinity and difference of surface and bottom salinity (black line), calculated for the input parameters derived in section 3.3 for station 1.

the observations. The magnitude of SPM concentration (Fig. 7b) is in the right order of magnitude and, most importantly, the enhanced values during flood are well represented. All key features of the observations, tidal asymmetry and periodic salinity stratification, appear in the model output, and their interaction and effects on the sediment transport can now be investigated in detail in the following section.

4.2. Drivers for SPM transport

To determine the isolated effect of tidal asymmetries and periodic stratification on the suspended sediment transport in this context, two additional model calculations are performed. In the 'symmetric' scenario, a purely sinusoidal forcing for surface elevation and velocity is used, together with the parameterized salinity stratification described in section 3.3. In the 'no salinity' scenario, the tidal current and surface elevation are asymmetric, but salinity was kept

constant, both in the vertical and over time. Note that a model scenario with constant salinity and symmetric tides would be trivial, as the residual current and residual transport of SPM vanish in this case.

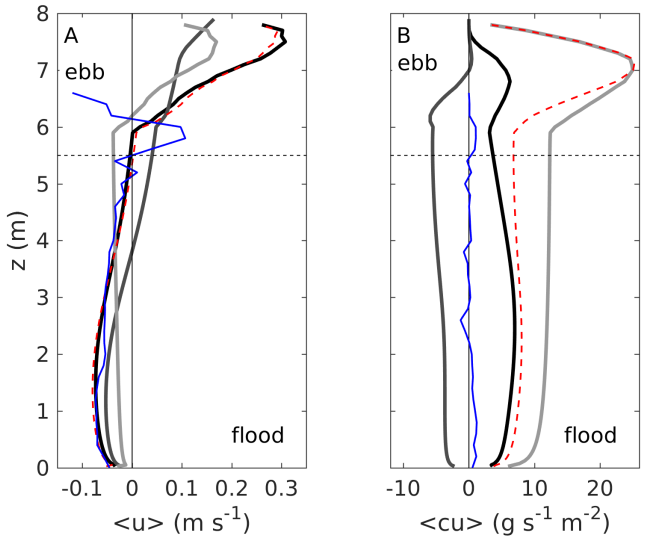

Figure 8: (a) Residual current and (b) residual SPM flux calculated for the three different scenarios described above. The black line displays the results for the 'realistic' forcing scenario, light and dark gray the 'no salinity' and the 'symmetric' scenario, respectively. Blue lines are the observational data from cruise 2, station 1. The red dashed lines denote the sum of the two gray profiles, respectively. The horizontal dashed line marks the low water level.

In Fig. 8, the residual current and SPM flux are displayed for the different model scenarios. The profiles obtained with the realistic scenario (black line) represent well the observed profiles, displayed in Fig. 3. The two-layered structure of the residual current is well reproduced, with the near bottom current pointing in the ebb direction. The SPM transport in the flood direction is consistent with the observations (see Fig. 3b), but notably higher than the measured transport for cruise 2, station 1. The reason for this is the overestimation of the difference between the maximal SPM concentration during ebb and flood phase in the model, which was not very pronounced during measurements at station 1 during cruise 2. In the upper part of the water column, where water is only

present during high tide, sediment transport is more pronounced in the flood direction. This is easily explained by the asymmetry in SPM concentration especially near the surface, where concentrations are greatly enhanced during the flood period (see Fig. 7b).

Remarkable are the effects of asymmetric tide and salinity variability on the residual current. Both the asymmetry and the periodic stratification induce a residual near-bottom current in the ebb direction of comparable magnitude. The similar shape of the current profiles for the realistic scenario (Fig. 8a, black line) and the scenario with symmetric tide (dark gray line) imply that the periodic stratification is the main factor determining the residual current, and the asymmetric tide merely causes a nearly constant shift of the profile in the direction of the elongated ebb. Adding the two profiles (red dashed line) nearly perfectly reproduces the profile obtained when combining both effects, implying that tidal asymmetry and periodic stratification act independently of each other on the residual current.

The residual SPM flux (Fig. 8b) reveals a different picture. The absence of a periodic salinity stratification approximately doubles the near bottom transport in flood direction (more import), whereas the absence of tidal asymmetries reverses the transport to the ebb direction (export). Also, the two SPM transport mechanisms seem to interact non-linearly with each other, as the combined transport profile strongly deviates from the result for the realistic run. To examine this in detail, the temporal evolution of the suspended matter concentration for all scenarios is displayed in Fig. 9.

The variability of suspended sediment concentration is qualitatively similar for the 'realistic' and the 'no salinity' scenario (Fig. 9a, c). In the absence of salinity gradients (Fig. 9c), the enhanced vertical mixing is reflected in the higher peak sediment concentrations and also higher concentrations during phases where no erosion takes place (at low current speeds). This directly explains the larger transport visible in Fig. 8b (light gray and black lines). In the scenario with a symmetric tidal current, SPM concentrations are higher during the ebb phase (Fig. 9,b). The periodic stratification established during flood

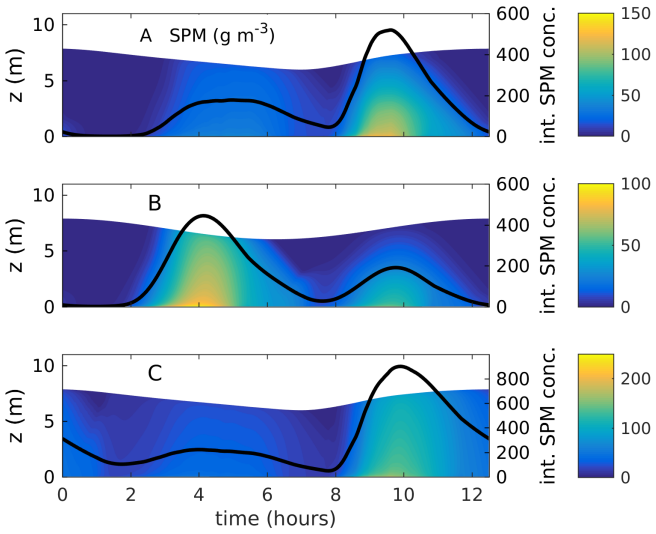

Figure 9: Temporal evolution of SPM concentration and integrated SPM concentration for (a) the realistic scenario (reprint from Fig. 7b for better comparison), (b) the symmetric scenario and (c) the constant salinity scenario. Please note the different scales.

leads to a reduction of the maximal vertically integrated sediment concentration of 60 % compared to the maximal value during ebb. However, the magnitude of sediment in the water column is approximately the same as in the realistic scenario (Fig. 9a). The same model study using the parameters derived for station 2 (Fig. S12) reveals a similar distribution of residual currents and SPM fluxes.

4.3. Effects of Periodic Stratification

For a further examination of the competing effects of tidal asymmetries and periodic stratification, the influence of a gradually increasing stratification strength on the integrated SPM flux is calculated in this section. Therefore, the 'realistic' forcing scenario was combined with a periodic salinity stratification as described in section 3.3, with maximal values of ΔS ranging from zero (the case with no salinity variability) to 10. This study was performed for both stations (always using the same erosion constant of $\alpha_e = 1.5 \times 10^{-6}$ kg s^{-1} m^{-2} for an

easier comparison), and for each scenario, the vertically integrated tidal mean SPM flux was calculated. The results are displayed in Fig. 10. As expected, enhanced salinity stratification reduces the total transport of suspended matter, but this relation is not linear: In the model setup for station 1, each increase of 1 in maximal top to bottom salinity stratification reduces the transport of SPM by approximately 20 %. A change in water depth, which is the main difference between station 1 (7 m) and station 2 (4 m) generally enhances or decreases the transport, but the qualitative relation between salinity stratification and SPM transport remains unchanged.

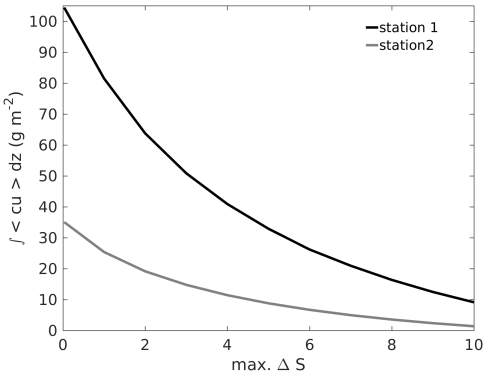

Figure 10: Integrated residual SPM flux as a function of surface to bottom salinity difference as described in Eq. 5 for both stations.

5. Discussion

In general, the residual fluxes of water (and sediment) in the Wadden Sea reveal a strong variability due to wind conditions [12, 24]. This is also reflected in the data set investigated here: the residual current measured during the presence of high wind speeds (cruise 1, station 2) differs substantially from the other measurements. As wind forcing is not included in the model, it should be kept in mind that this variability cannot be reproduced and the following discussion is only valid assuming small to intermediate wind speeds.

Fresh water was discharged through the sluice in Kornwerderzand prior to every measurement, except for the first one (station 1) on cruise 2. The periodic stratification that is nevertheless established during flood in this case without prior freshwater discharge (Fig. S3) indicates the permanent presence of fresh water influence in the vicinity of the study area. This is supported by the findings in [12], where, among other things, the fate of sluice discharge in the Western Dutch Wadden Sea (WDWS) was investigated: Fresh water from Kornwerderzand is distributed in the whole WDWS, with the largest volumes located in the channels. The flushing time for the discharged water from Kornwerderzand, i.e. the time it would take to export the available fresh water through the tidal inlets or the watershed in the east at the tidally averaged outflow rate, was found to be approximately 16 days [12]. It is therefore reasonable to assume that the tidal dynamics in the investigated Kimstergat channel are permanently under the influence of fresh water discharged at Kornwerderzand.

Fresh water is also discharged through the port of Harlingen. The annual mean discharge of less than 5 m^3 s^{-1} here is much smaller than in Kornwerderzand, but in the direct vicinity of the study site [12].

With no strong winds and sufficient fresh water discharge, the patterns of the residual transport in the Kimstergat can be derived from the observations and explained by the model results: The near bottom residual current is in all cases directed in the ebb direction, not only because of the periodic salinity stratification but also because of the asymmetric tidal current. Both effects are of comparable magnitude and add up to the total residual current. Nevertheless, the greatly enhanced SPM concentrations during the flood phase cause a transport of sediment in the flood direction, which is visible in all observational data sets. Model results suggest that the magnitude of the salinity stratification during the flood phase affects the sediment transport: the higher the stratification, the lower the transport. This is reasonable, as the upward mixing of suspended sediment is generally hindered by stratification [6]. The only observations that did not show a periodic salinity stratification coincide with times of very high wind speeds (wind from the south-west), and are therefore not comparable to

the modeled data.

6. Conclusions

In this study, observational data from three cruises were compared to different scenarios of an idealized numerical model to investigate the key features of residual transports in the Kimstergat channel. One important finding is that in the vicinity of a large fresh water source near the mouth of the channel a periodically occurring vertical salinity stratification is established during the flood phase and destroyed during the ebb phase. This periodic stratification is inverse of what is normally observed in estuaries. The model results show that without salinity gradients, the import of SPM into the channel would be much larger, approximately doubled. In other words, the salinity gradients actually diminish the import, contrary to normal estuarine behavior. Despite the counteracting effect of these inverse estuarine dynamics, there is still an import of SPM because of tidal asymmetries and a resulting higher SPM concentration during flood. Together with the onshore transport observed towards the end of the channel, these transport patterns support the idea of the Mud Motor and suggest that sediment deposited in the channel will eventually be transported towards the adjacent salt marshes, but that the effect would have been even stronger without a freshwater source at the mouth of the channel.

The advection of fresh water into the mouth of a channel or estuary is certainly not unique. It has been observed e.g. in the Chesapeake Bay system and might be common in subestuary-estuary interactions [11]. Also, the discharge of sluices, sea locks or other large fresh water sources can be pushed into nearby channels with the flood current, as it is described in this study. Whether or not the advection of fresh water occurs intermittent or continuously, the resultant periodic salinity stratification can induce a residual SPM transport. This study shows that non-continuous sluice discharge results in a continuously occurring periodic stratification in a tidal channel at a distance of over 10 km. Consequently, in the absence of pronounced tidal asymmetries, fresh water advected

into the mouth of a channel (or estuary) several kilometers away from a the fresh water source could create an export from the channel and cause sediment accumulation at its mouth.

An extension of the idealized model to account for wind and wave effects, or even a regional three-dimensional model could help to understand sediment transport patterns in the Kimstergat channel in further detail. Additionally, an analysis of the stratification effects on turbulence, both through observational data and numerical modeling, would provide useful information to work with in the future.

Acknowledgements

This work was funded by the STW project "Sediment for the salt marshes: physical and ecological aspects of a mud motor" (grant number 13888). We like to acknowledge the crew of the RV Navicula, Janine Nauw, Borja Aguiar Gonzàlez, for technical assistance, Eric Wagemaakers, Jaco de Smit for the translation of Dutch literature and Manuel Ruiz-Villarreal for his explanations on the Rias Baixas system. Two anonymous reviewers provided valuable suggestions for the improvement of this manuscript. Computations were carried out with the General Ocean Turbulence Model (GOTM, www.gotm.net) with the SPM component implemented using the Framework for Aquatic Biogeochemical Models (FABM, www.sf.net/projects/fabm).

References

[1] J. H. Simpson, J. Brown, J. Matthews, G. Allen, Tidal straining, density currents, and stirring in the control of estuarine stratification, Estuaries and Coasts 13 (2) (1990) 125–132.

[2] P. MacCready, W. R. Geyer, Advances in estuarine physics, Annual Review of Marine Science 2 (2010) 35–58.

[3] H. Burchard, R. D. Hetland, Quantifying the contributions of tidal straining and gravitational circulation to residual circulation in periodically stratified tidal estuaries, Journal of Physical Oceanography 40 (6) (2010) 1243–1262.

[4] D. A. Jay, J. D. Musiak, Particle trapping in estuarine tidal flows, Journal of Geophysical Research: Oceans 99 (C10) (1994) 20445–20461.

[5] H. Burchard, H. M. Schuttelaars, W. R. Geyer, Residual sediment fluxes in weakly-to-periodically stratified estuaries and tidal inlets, Journal of Physical Oceanography 43 (9) (2013) 1841–1861.

[6] M. E. Scully, C. T. Friedrichs, The influence of asymmetries in overlying stratification on near-bed turbulence and sediment suspension in a partially mixed estuary, Ocean Dynamics 53 (3) (2003) 208–219.

[7] M. Lavın, V. Godınez, L. Alvarez, Inverse-estuarine features of the Upper Gulf of California, Estuarine, Coastal and Shelf Science 47 (6) (1998) 769–795.

[8] M. deCastro, M. Gomez-Gesteira, I. Alvarez, R. Prego, Negative estuarine circulation in the Ria of Pontevedra (NW Spain), Estuarine, Coastal and Shelf Science 60 (2) (2004) 301–312.

[9] P. A. Díaz, M. Ruiz-Villarreal, L. Velo-Suárez, I. Ramilo, P. Gentien, M. Lunven, L. Fernand, R. Raine, B. Reguera, Tidal and wind-event variability and the distribution of two groups of Pseudo-nitzschia species in an upwelling-influenced Ría, Deep Sea Research Part II: Topical Studies in Oceanography 101 (2014) 163–179.

[10] E. D. Barton, J. Largier, R. Torres, M. Sheridan, A. Trasviña, A. Souza, Y. Pazos, A. Valle-Levinson, Coastal upwelling and downwelling forcing of circulation in a semi-enclosed bay: Ria de Vigo, Progress in Oceanography 134 (2015) 173–189.

[11] D. Hayward, C. S. Welch, L. W. Haas, York river destratification: an estuary-subestuary interaction, Science 216 (4553) (1982) 1413–1414.

[12] M. Duran-Matute, T. Gerkema, G. J. De Boer, J. J. Nauw, U. Gräwe, Residual circulation and freshwater transport in the Dutch Wadden Sea: a numerical modelling study, Ocean Science 10 (4) (2014) 611–632.

[13] E. van Eekelen, M. Baptist, P. Dankers, B. Grasmeijer, T. van Kessel, D. van Maren, Muddy waters and the Wadden Sea harbours.

[14] E. Elias, A. Van der Spek, Z. B. Wang, J. De Ronde, Morphodynamic development and sediment budget of the Dutch Wadden Sea over the last century, Netherlands Journal of Geosciences 91 (03) (2012) 293–310.

[15] EPSG, Geomatics Guidance note number 7, part 2.

[16] J. D'Errico, inpaint nans, MATLAB Central File Exchange, Retrieved March 21, 2017.

[17] F. J. Millero, R. Feistel, D. G. Wright, T. J. McDougall, The composition of Standard Seawater and the definition of the Reference-Composition Salinity Scale, Deep Sea Research Part I: Oceanographic Research Papers 55 (1) (2008) 50–72.

[18] P. Sprent, Applied nonparametric statistical methods, 2nd edn., Chapman and Hall (London), 1993.

[19] L. M. Merckelbach, H. Ridderinkhof, Estimating suspended sediment concentration using backscatterance from an acoustic Doppler profiling current meter at a site with strong tidal currents, Ocean Dynamics 56 (3-4) (2006) 153–168.

[20] T. Gerkema, J. Nauw, C. van der Hout, Measurements on the transport of suspended particulate matter in the Vlie Inlet, Netherlands Journal of Geosciences 93 (3) (2014) 95.

[21] L. Umlauf, H. Burchard, Second-order turbulence closure models for geophysical boundary layers. A review of recent work, Continental Shelf Research 25 (7) (2005) 795–827.

[22] H. Burchard, G. Flöser, J. V. Staneva, T. H. Badewien, R. Riethmüller, Impact of density gradients on net sediment transport into the Wadden Sea, Journal of Physical Oceanography 38 (3) (2008) 566–587.

[23] Y. Cheng, V. Canuto, A. Howard, An improved model for the turbulent PBL, Journal of the Atmospheric sciences 59 (9) (2002) 1550–1565.

[24] M. Sassi, M. Duran-Matute, T. van Kessel, T. Gerkema, Variability of residual fluxes of suspended sediment in a multiple tidal-inlet system: the Dutch Wadden Sea, Ocean Dynamics 65 (9-10) (2015) 1321–1333.

[25] K. Schulz, L. Umlauf, Residual transport of suspended material by tidal straining near sloping topography, Journal of Physical Oceanography 46 (7) (2016) 2083–2102.

[26] M. T. Stacey, J. P. Fram, F. K. Chow, Role of tidally periodic density stratification in the creation of estuarine subtidal circulation, Journal of Geophysical Research: Oceans 113 (C8).

Supplementary material

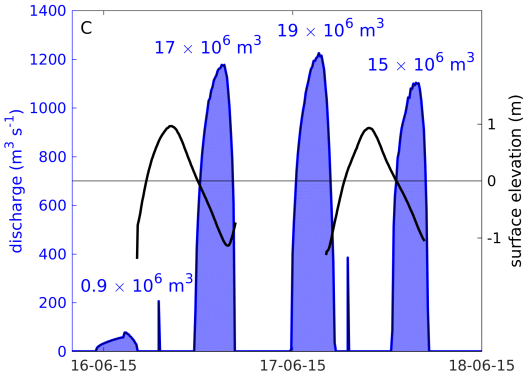

Figure S1: Discharge of the sluice in Kornwerderzand (blue line) and relative surface elevation from two consecutive days of measurements (black lines, see next section for details on the deployments) over two days. Blue numbers refer to the integrated discharge in the shaded areas below, respectively. Data were provided by the Dutch governmental organization Rijkswaterstaat.

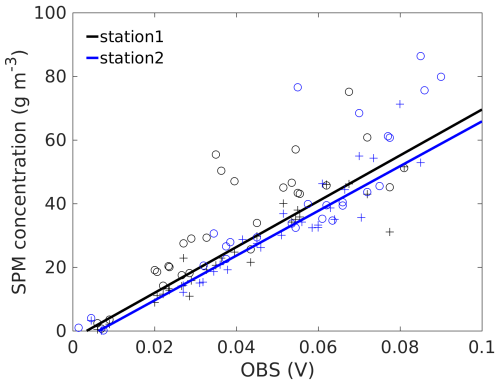

Figure S2: Correlation of SPM concentration and OBS values and the linear regressions obtained with the Theil-Sen method for both stations during cruise 3. Crosses refer to measurements near the surface, circles to measurements near the bottom.

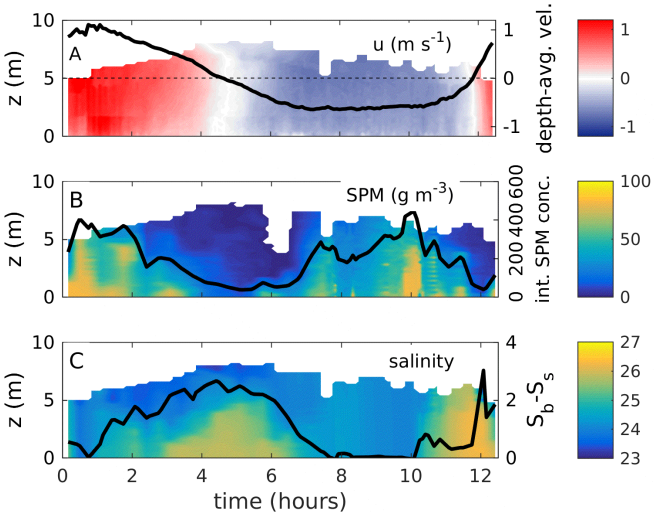

Figure S3: As Fig. 2, but for cruise 1, station 1.

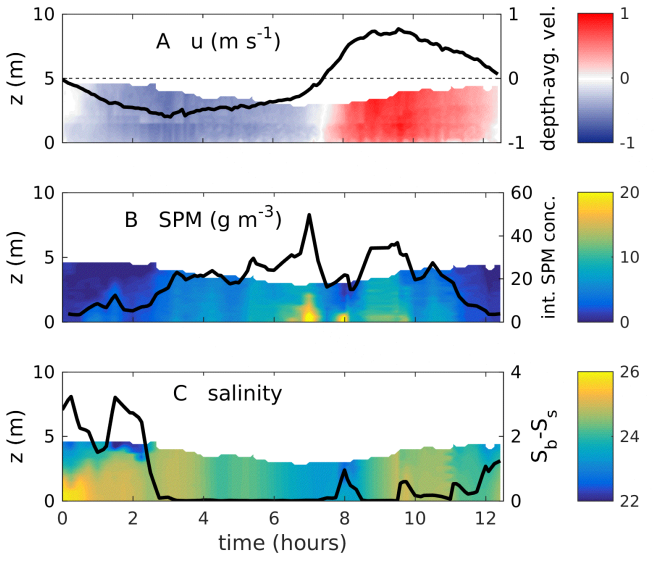

Figure S4: As Fig. 2, but for cruise 3, station 1.

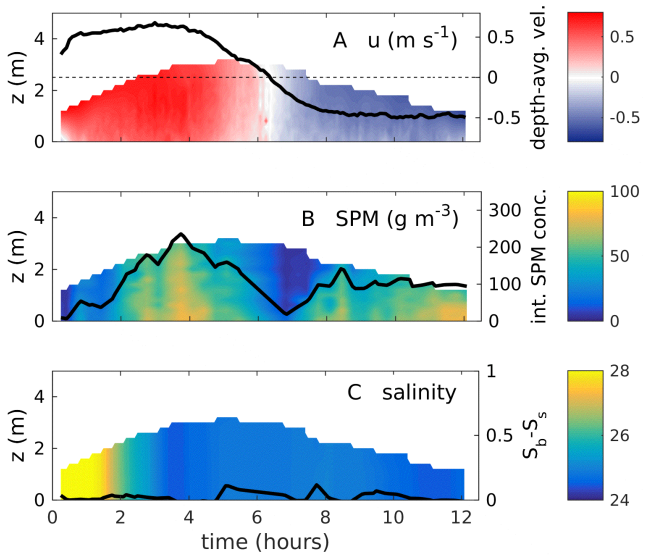

Figure S5: As Fig. 2, but for cruise 1, station 2.

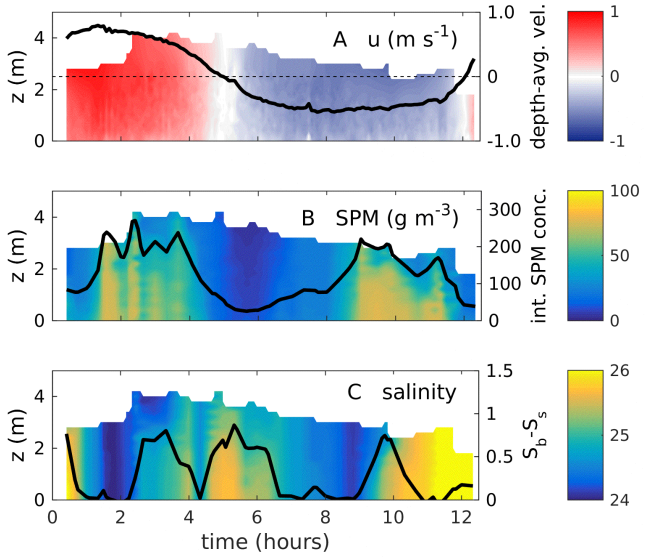

Figure S6: As Fig. 2, but for cruise 2, station 2.

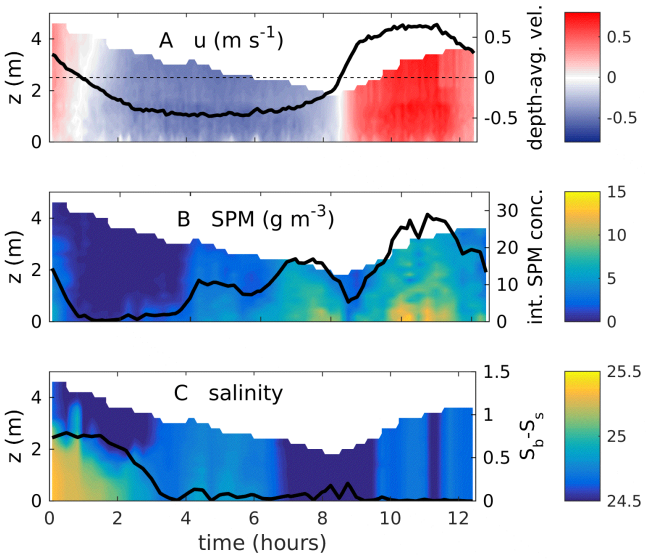

Figure S7: As Fig. 2, but for cruise 3, station 2.

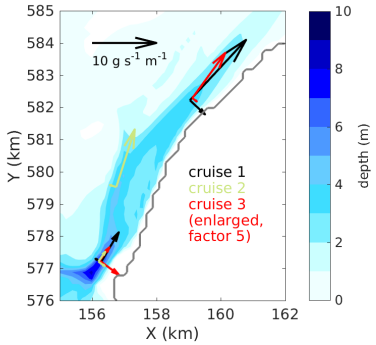

Figure S8: Visualization of the along- and cross-channel integrated sediment flux for all cruises and both stations summarized in Tab. 3. Note that the values obtained during cruise 3 are in reality 5 times smaller, but were scaled up here for better visibility.

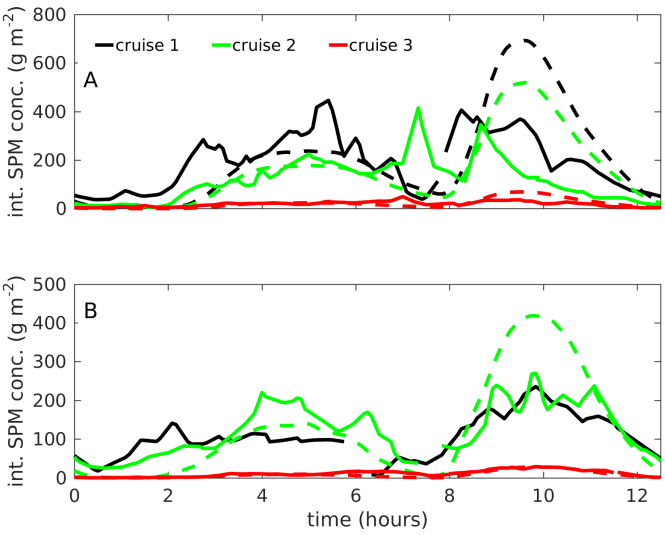

Figure S9: Observed (solid lines) and modeled (dashed lines) integrated sediment concentrations at (a) station 1 and (b) station 2 for all cruises, aligned again with the onset of ebb.

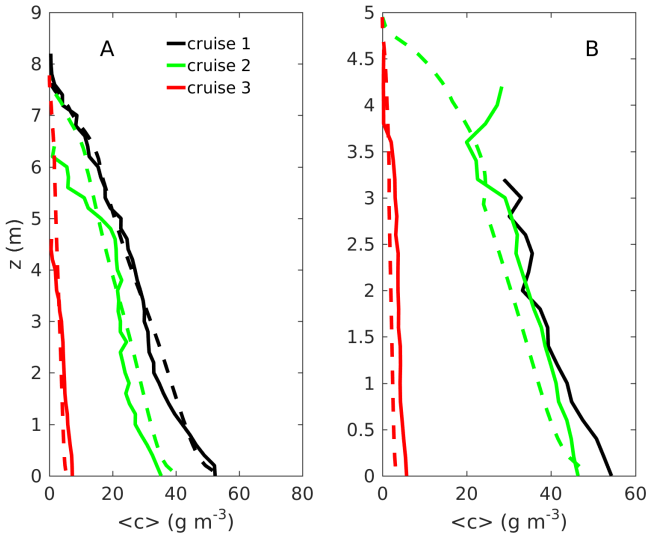

Figure S10: Observed (solid lines) and modeled (dashed lines) tidally averaged sediment concentrations at (a) station 1 and (b) station 2 for all cruises.

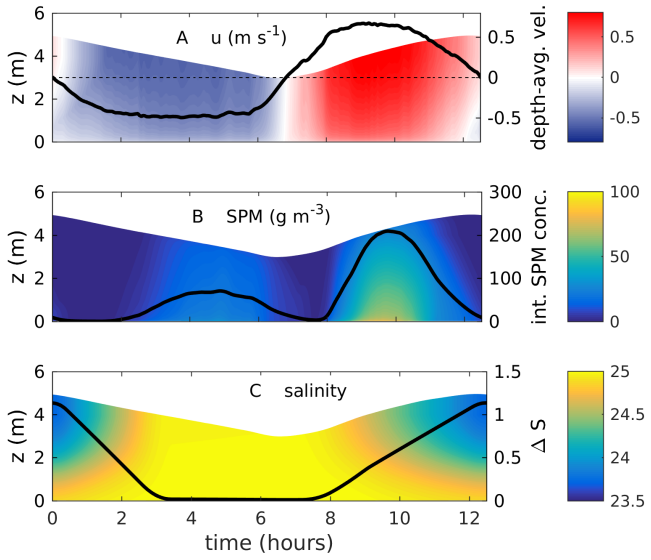

Figure S11: Temporal evolution of (a) the along-channel and depth-averaged (black line) velocity, (b) SPM concentration and integrated concentration (black line), and (c) salinity and difference of surface and bottom salinity (black line), calculated for the input parameters derived in section 3.3 for station 2, with an erosion constant of 1.5×10^{-6} kg s^{-1} m^{-2}.

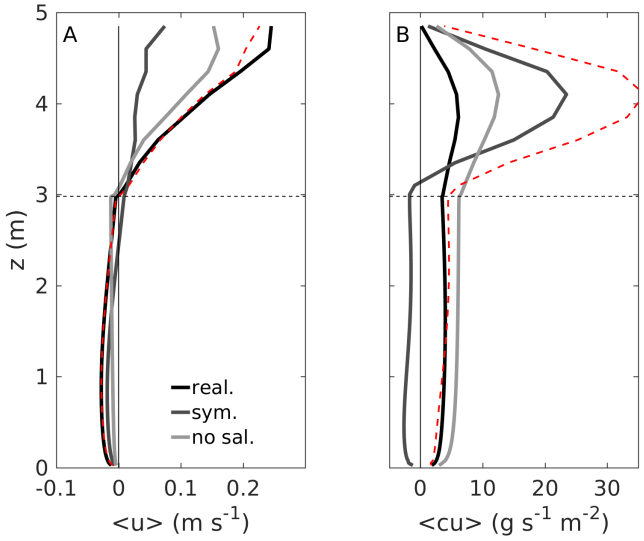

Figure S12: As Fig. 8, but for station 2: (a) Residual current and (b) residual SPM flux calculated for the three different scenarios. The red dashed lines denote the sum of the two gray profiles, respectively. The horizontal dashed line marks the low water level.

Estuarine, Coastal and Shelf Science 207 (2018) 510

Contents lists available at ScienceDirect

Estuarine, Coastal and Shelf Science

journal homepage: www.elsevier.com/locate/ecss

Corrigendum

Corrigendum to 'An inversion of the estuarine circulation by sluice water discharge and its impact on suspended sediment transport.'[Estuarine, Coastal and Shelf Science 200 (2018) 31-40]

Kirstin Schulz*, Theo Gerkema

NIOZ Netherlands Institute for Sea Research, Department of Estuarine and Delta Systems, and Utrecht University, P.O. Box 140, 4400 AC Yerseke, The Netherlands

The authors regret the following two incorrect statements in the paper:

1. The yearly amount of dredged sediment in the port of Harlingen is 1.3 million m^3. The amount we mentioned in the introduction, 200.000 m^3, refers to the part that is brought to the alternative spreading location.
2. Due to a scripting error, the amplification factors concerning the voltage output of the optical backscatter sensors, which were different for different cruises, were not included correctly. As a result, the suspended particulate matter (SPM) concentrations shown in the paper were too low by a factor of 4 for cruises 1 and 2, and by a factor of 5 for cruise 3. This does not affect the principal conclusions of the paper. To get the corrected values, the SPM concentrations and fluxes in the figures, the transport rates summarized in Table 3, and the erosion constants for the SPM model have to be multiplied by the respective factors. Fig. 3, in which vertical profiles SPM fluxes for all cruises were plotted in one figure, is the only result that was qualitatively wrong. For this reason, it is reprinted in this corrigendum.

The data is available at doi 10.4121/uuid:762ae98e-8ba8-47e8-b6cb-c983cd296167.

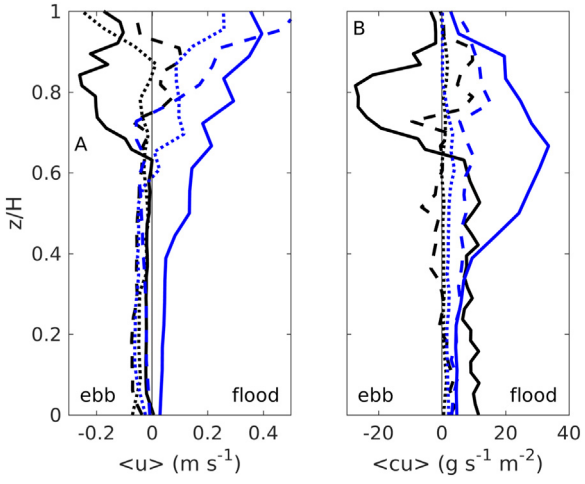

Fig. 3. Vertical profiles of (a) the residual current and (b) the residual SPM flux, for all cruises. Solid lines refer to measurements from cruise 1, dashed line to cruise 2 and dotted lines to cruise 3, respectively. Black lines refer to station 1, blue lines to station 2.

The authors would like to apologise for any inconvenience caused.

DOI of original article: http://dx.doi.org/10.1016/j.ecss.2017.09.031
* Corresponding author.
E-mail address: kirstin.schulz@nioz.nl (K. Schulz).

https://doi.org/10.1016/j.ecss.2018.05.003

0272-7714/ © 2018 Elsevier Ltd. All rights reserved.